ACS APPLIED MATERIALS & INTERFACES

www.acsami.org

Research Article

Capping Layers to Improve the Electrical Stress Stability of MoS_2 Transistors

James L. Doherty, Steven G. Noyce, Zhihui Cheng, Hattan Abuzaid, and Aaron D. Franklin*

Cite This: *ACS Appl. Mater. Interfaces* 2020, 12, 35698–35706

Read Online

ACCESS | Metrics & More | Article Recommendations | Supporting Information

ABSTRACT: Two-dimensional (2D) materials offer exciting possibilities for numerous applications, including next-generation sensors and field-effect transistors (FETs). With their atomically thin form factor, it is evident that molecular activity at the interfaces of 2D materials can shape their electronic properties. Although much attention has focused on engineering the contact and dielectric interfaces in 2D material-based transistors to boost their drive current, less is understood about how to tune these interfaces to improve the long-term stability of devices. In this work, we evaluated molybdenum disulfide (MoS_2) transistors under continuous electrical stress for periods lasting up to several days. During stress in ambient air, we observed temporary threshold voltage shifts that increased at higher gate voltages or longer stress durations, correlating to changes in interface trap states (ΔN_{it}) of up to 10^{12} cm^{-2}. By modifying the device to include either SU-8 or Al_2O_3 as an additional dielectric capping layer on top of the MoS_2 channel, we were able to effectively reduce or even eliminate this unstable behavior. However, we found this encapsulating material must be selected carefully, as certain choices actually amplified instability or compromised device yield, as was the case for Al_2O_3, which reduced yield by 20% versus all other capping layers. Further refining these strategies to preserve stability in 2D devices will be crucial for their continued integration into future technologies.

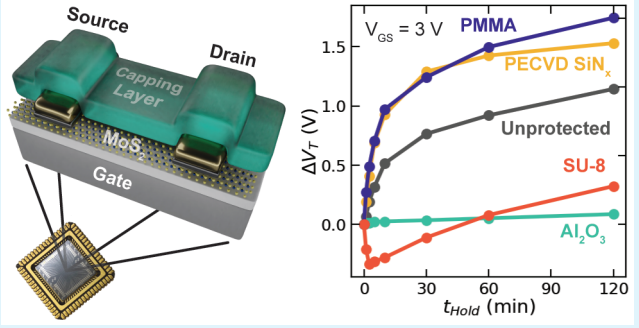

KEYWORDS: *2D materials, molybdenum disulfide, field-effect transistor, electrical stress, threshold voltage, passivation*

INTRODUCTION

Transition metal dichalcogenides (TMDs) are a class of atomically thin two-dimensional (2D) nanomaterials with many promising applications in electronics.[1,2] In particular, molybdenum disulfide (MoS_2) is a naturally abundant TMD with a large bandgap, making it a prime candidate for the channel material in future low-power field-effect transistors (FETs).[3−6] Scaled MoS_2 FETs commonly demonstrate impressive on−off current ratios and subthreshold swing, but obtaining consistently high drive current remains challenging.[7−9] One key issue is the highly variable room-temperature field-effect mobility commonly observed in scaled MoS_2 FETs.[10,11] While some variation could arise from imperfections in mobility extraction techniques, it is possible that much of this variation is due to disorder or charged impurities around the MoS_2 channel. Many methods have been investigated to reduce disorder, such as modification of the substrate chemistry underneath the channel,[12−14] full encapsulation of the channel with a high-k dielectric or 2D insulator such as hexagonal boron nitride,[15−18] and repair of sulfur vacancy defects in the MoS_2 lattice.[19,20] Recent MoS_2 FETs built on corrugated substrates even exceeded many projected mobility limits at room temperature,[21] indicating that the dielectric interfaces to MoS_2 can be engineered to resolve and even reverse the mobility degradation issue. Further improvements at the dielectric interface will be crucial to the continued development of scaled MoS_2 transistors.

In addition to scaled transistors, larger form-factor MoS_2 FETs have been explored for their application in photovoltaic cells,[22,23] nonvolatile memories,[24,25] and gas sensors.[26−28] Although resolving mobility variability is important for devices used in these applications, it is also critical for these devices to function without significant degradation over long operating lifetimes. Therefore, it is important for the structure of these devices to be designed with stability in mind. Many MoS_2 FETs studied use a simple back-gated design so that the surface of the MoS_2 channel is exposed. It has been shown previously that these devices are susceptible to the adsorption of oxygen and water molecules,[29,30] which contribute to interface trap density[31] and cause increased hysteresis.[32−35] When these devices are biased at a particular gate voltage for

Received: May 11, 2020
Accepted: July 13, 2020
Published: July 27, 2020

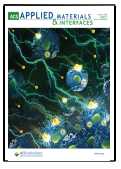

https://dx.doi.org/10.1021/acsami.0c08647
ACS Appl. Mater. Interfaces 2020, 12, 35698−35706

extended periods of time, the gradual accumulation or depletion of charge in these interface trap states causes the device threshold voltage (V_T) to temporarily shift.[36,37] These transient effects are highly undesirable, and to mitigate them it is necessary to identify effective strategies for preventing molecular adsorption onto the surface of MoS_2.

One strategy for mitigating the impact of ambient exposure is the encapsulation of the MoS_2 with additional layers of protection on top of the channel. Although there have been many studies to date investigating a wide variety of capping layers on MoS_2 FETs, their effectiveness at preventing molecular adsorption has received comparatively little attention as most have focused on how modification of the MoS_2−dielectric interface can boost field-effect mobility.[10,13,15−17] Studies of polymer capping layers to protect MoS_2 FETs from the ambient have focused on fluorinated CYTOP[38] and p(V4D4-*co*-CHMA) copolymers,[39] although neither one appeared to completely stabilize the threshold voltage under extended periods of bias stress. One group has also studied the effects of bias stress on MoS_2 FETs encapsulated by hexagonal boron nitride (h-BN)[40] and ALD-grown alumina (Al_2O_3).[41] Both of these approaches significantly suppressed hysteresis in the devices, although both still allowed V_T shifts under certain conditions. Finally, a more recent study incorporated a 3 nm-thick TiO_2 interfacial encapsulation layer in order to study electrical stress and the role of Fermi-level pinning at the contacts.[42] However, note that none of these reports have systematically examined more than one capping material for the comparative impact of electrical stress on device stability. Unfortunately, due to variations in device fabrication and characterization methodologies across the various studies, it is challenging to compare the results and identify the definitive strengths and weaknesses of diverse passivation approaches. A study of multiple passivation materials using consistent characterization techniques would reveal which passivation material properties impact the physical mechanisms that drive molecular adsorption and would guide efforts across applications with different material integration requirements.

Here, we investigated the effects of gate- and drain-bias stress on MoS_2 field-effect transistors capped with a variety of passivation layers, including a study of the impact of the electrical stress on device operation under ambient air conditions. We further explored the sensitivity of the devices to variations in stress time and voltage. After baseline device characterization, MoS_2 channels were covered with a variety of capping layers, including poly(methyl methacrylate) (PMMA), SU-8 photoresist, silicon nitride (SiN_x), and aluminum oxide (Al_2O_3). The hydrophilic PMMA layer proved to be ineffective passivation, while the much thicker and hydrophobic SU-8 film provided notable improvements, particularly in short-term stress tests. Devices capped with SiN_x were surprisingly unstable, likely due to defects introduced during film deposition. Only the Al_2O_3-passivated devices demonstrated full stability with no discernible threshold voltage shift after days of continuous bias; yet, the atomic layer deposition (ALD) process for the Al_2O_3 also resulted in the lowest device yield compared to the other passivation layers. These results shed light on the role of interface control and passivation material selection in the electrical stability and yield of MoS_2-based devices, highlighting some key trade-offs.

RESULTS AND DISCUSSION

The MoS_2 FETs were fabricated using conventional lithography and thin-film deposition techniques. MoS_2 flakes (whose molecular diagram is shown in Figure 1A) were mechanically

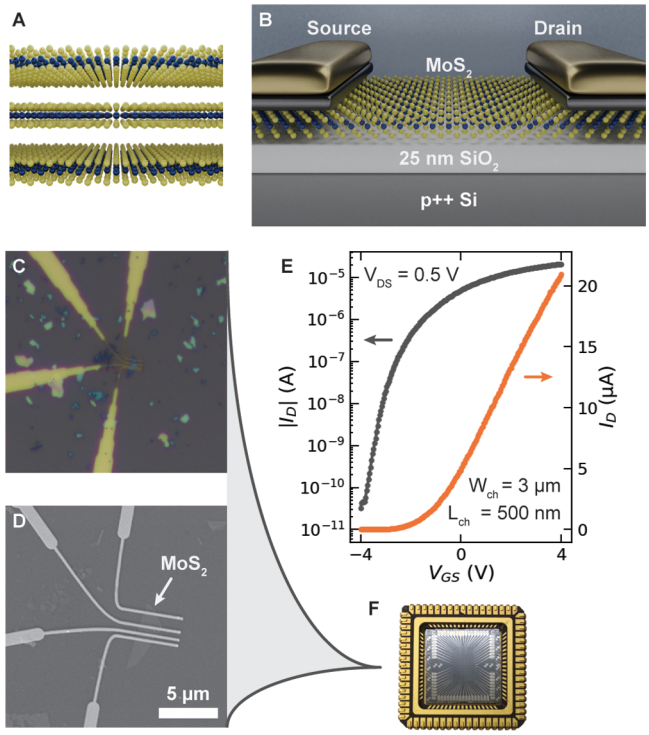

Figure 1. MoS_2 FET device structure and wire-bonding for long-term characterization. (A) Molecular diagram of the van der Waals-layered structure of MoS_2. (B) Device schematic of a back-gated MoS_2 FET with 10 nm Ni (topped with 20 nm Pd) source/drain contacts. (C) Optical microscope and (D) SEM image of a set of three devices with different channel lengths. (E) Typical transfer and subthreshold characteristics of a device measured in ambient conditions. (F) Chip installed and wire-bonded into chip carrier for testing at the end of fabrication.

exfoliated from a bulk crystal (2D Semiconductors Inc.) onto highly doped p++ silicon wafers with a 25 nm thick thermal oxide. Thin multilayer MoS_2 flakes (approximately 4−8 nm thick, see Figure S1 in the Supporting Information) were identified by an optical contrast technique developed previously,[43,44] after which metal contacts were defined by electron-beam lithography, electron-beam evaporation, and metal lift-off. A schematic of the finished device is shown in Figure 1B with optical and SEM images of typical devices shown in Figure 1C,D. Electrical characterization (Figure 1E) was performed using Keysight B2900A source measure units under ambient conditions unless otherwise specified. To facilitate extensive long-term testing, many completed chips were wire-bonded to ceramic packages (Figure 1F) that fit the sockets on custom measurement systems, as previously described.[45] A full description of fabrication and characterization procedures is available in the Supporting Information along with a detailed extraction of performance metrics for all devices studied (see Table S1, Figures S2−S8). Of particular note in Table S1 are the "initial device yield" percentages recorded for every chip, showing that yield improved from ∼30% up to ∼81% by several simple fabrication improvements including using sufficiently wide metal lines for signal routing,

https://dx.doi.org/10.1021/acsami.0c08647
ACS Appl. Mater. Interfaces 2020, 12, 35698−35706

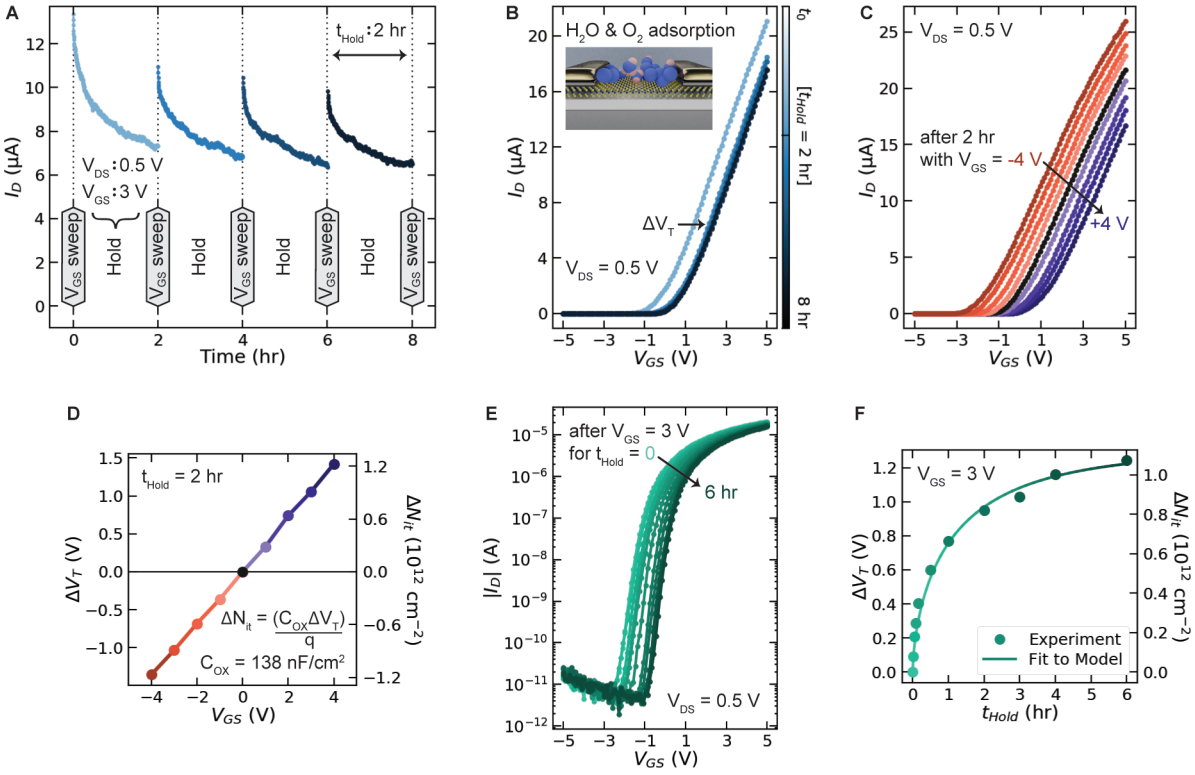

Figure 2. Susceptibility of nonpassivated MoS_2 FETs to molecular adsorption from ambient air conditions. (A) Long-term biasing of a MoS_2 FET in ambient air at V_{DS} = 0.5 V and V_{GS} = 3 V with periodic interruptions every 2 h to measure transfer characteristics (V_{GS} sweep). (B) Transfer curves measured throughout the experiment in (A), showing a positive threshold voltage shift as a result of the accumulation of adsorbed species on the surface of the MoS_2 channel. (C) Transfer curves measured after 2 h of biasing at a static gate voltage; tested for V_{GS} = −4 V to +4 V in increments of 1 V. (D) Magnitude of threshold voltage shifts extracted from (C), showing equal and opposite shifts for positive and negative V_{GS} bias voltages, where the dual axis shows the corresponding estimated change in interface trap occupancy. (E) Transfer curves measured after biasing at a static gate voltage of V_{GS} = 3 V for hold times ranging up to t_{Hold} = 6 h. (F) Magnitude of threshold voltage shifts and change in interface trap occupancy extracted from (E), showing their fit to a stretched exponential bias-stress model. L_{ch} = 500 nm and W_{ch} = 3 μm for this device.

avoiding very thick MoS_2 flake deposits, and limiting electrical connection between devices so that individual failures are isolated. The total yield of MoS_2 devices in this study finished at 49% (100 out of 204 devices).

Prior to studying the influence of different capping layers on MoS_2 FET stability and performance, baseline back-gated devices were fully characterized. Because of previous reports[36,37] of the threshold voltage instability of MoS_2 transistors under bias stress, focus was given to this behavior in our devices. Figure 2A shows the results of an experiment in which a MoS_2 FET was held in the on-state with a drain voltage of V_{DS} = 0.5 V and a gate voltage of V_{GS} = 3 V for four consecutive time segments of length t_{Hold} = 2 h. Between bias-stress segments, the gate voltage was swept in order to extract the device characteristics shown in Figure 2B. From the initial device behavior, there is a positive threshold voltage shift (ΔV_T) in each of the other four measurements of the transfer characteristics. This simple experiment yields several important insights into the back-gated, nonpassivated MoS_2 FET operating in ambient air: (1) even though we applied constant drain and gate voltages, the drain current was not constant over time, changing by up to 45% from its initial value; (2) the drain current was changing because the threshold voltage of the device was changing; (3) the act of sweeping the gate voltage partially reset the threshold voltage shift in the device, but in the subsequent period of t_{Hold} the threshold voltage returned to the same terminal value; and (4) this process is repeatable, indicating that most of these effects are transient rather than permanent changes to the device. This unstable behavior was extremely consistent across many devices on different chips and wafers, including those with significantly different oxide thicknesses (see Figures S9−S11 for identical behavior in multilayer and monolayer devices on 90 nm SiO_2 substrates). In particular, the consistent behavior of the monolayer device (Figure S11) suggests that the stability issues observed in this work are dominated by extrinsic interfacial or dielectric-layer traps, since there is little apparent dependence on MoS_2 thickness.

Repeating the experiment shown in Figure 2A under low vacuum or in dry nitrogen conditions (see Figure S12) yielded a significant improvement in threshold voltage stability, consistent with previous reports.[37] This indicates that the dominant factor driving this behavior is the adsorption and desorption of oxygen and water molecules from the ambient air onto the surface of the MoS_2 channel. The impact of applying different polarity and magnitude of gate voltage to the device is seen in Figure 2C with the magnitudes of ΔV_T resulting from each bias stress V_{GS} shown in Figure 2D. There is a clear linear dependence of ΔV_T on the stress gate voltage that is symmetric for positive and negative gate voltages. This symmetry demonstrates that traps can just as easily be filled or emptied by applying a positive or negative gate voltage; however, interestingly the subthreshold swing (SS) is not symmetric, improving under negative stress and slightly degrading under positive stress (see Figure S13). Since SS degradation is associated with increased trap states, this

https://dx.doi.org/10.1021/acsami.0c08647
ACS Appl. Mater. Interfaces 2020, 12, 35698−35706

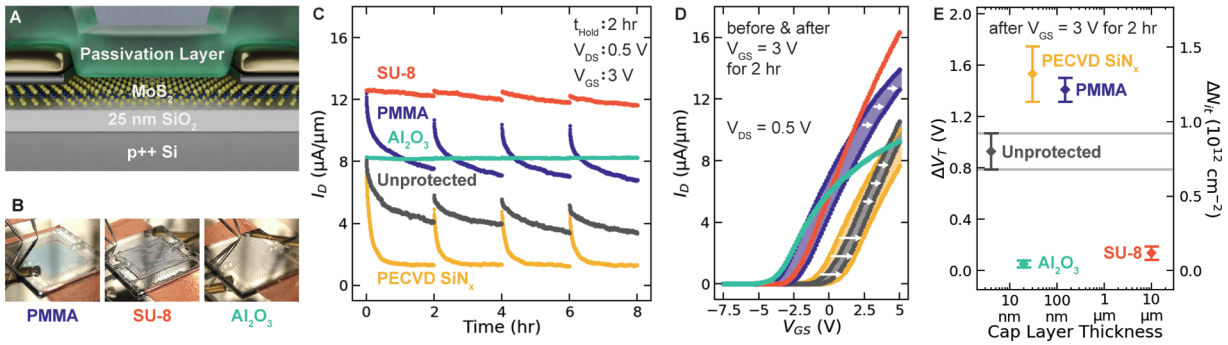

Figure 3. Accumulation of trapped charge with different passivation layers capping back-gated MoS_2 FETs when stressed for 2 h intervals. (A) Modified device schematic with passivation layer. (B) Photographs of chips coated in a variety of passivation layers. (C) Long-term biasing of MoS_2 FETs with different passivation layers, performed in ambient conditions with periodic interruptions every 2 h to measure transfer characteristics. (D) Transfer curves measured before and after the first 2 h of biasing shown in (C). (E) Magnitude of threshold voltage shift and corresponding approximate change in interface trap occupancy at the end of 2 h of biasing at V_{DS} = 0.5 V and V_{GS} = 3 V. Error bars show the mean and standard deviation of measurements from three different devices on each chip. L_{ch} = 500 nm for all devices shown.

suggests that positive stress is filling electron traps while negative stress is emptying those traps. The symmetry in ΔV_T is consistent with other reports of the nonpassivated MoS_2 FET,[37] but note that this behavior is not always symmetrical, as seen in CYTOP-passivated MoS_2 FETs which show larger ΔV_T under negative gate voltage stress.[38]

Although the observed ΔV_T is indicative of the behavior of trapped charges in these devices, V_T itself can vary widely across the device structures reported in different studies so it is preferable to use a different metric, such as change in interface trap occupancy (ΔN_{it}), that does not depend on the gate oxide thickness. By assuming a parallel plate capacitor model[15] for the oxide capacitance of the 2D FET structure, we are able to directly convert ΔV_T to the change in surface charge on the MoS_2 flake. A change in the surface charge during bias stress indicates that there has been a change in the density of electrons or holes occupying trap states (N_{it}) at the gate oxide interface. Therefore, we are able to use the inset equation in Figure 2D to compute an approximated change in N_{it} that corresponds to the observed ΔV_T, which is shown on the secondary axis of Figure 2D. The usefulness of ΔN_{it} as a figure of merit is highlighted more in the Supporting Information, which shows a device fabricated on a different substrate (90 nm SiO_2) experiencing the same stress as Figure 2C,D and exhibiting an almost identical relationship between gate bias and ΔN_{it} (see Figure S10). As a final note, for a sheet of charge with density 10^{12} cm^{-2}, the nearest-neighbor spacing was calculated to be approximately 10 nm, which was found to be a helpful metric for visualizing N_{it} (see Figure S14).

The final aspect of the baseline MoS_2 FETs that was investigated is the impact of stress time at a constant gate stress voltage, as shown in Figure 2E,F. Here we see that V_T evolves over time according to the same stretched-exponential model that has been widely used to model bias stress in MoS_2 transistors[39,46] as well as thin-film transistors based on zinc oxides[47,48] or organic semiconductors[49,50]

$$\Delta V_T(t) = V_0\left(1 - \exp\left[-\left(\frac{t}{\tau}\right)^{\beta}\right]\right)$$

where V_0 is the value of ΔV_T as $t \to \infty$ and τ is known as the relaxation time. The solid line in Figure 2F shows a fit to the experimental data with β of 0.65 and a relaxation time of 4500 s (1.25 h). Hence, the time scale over which these FETs should be analyzed for electrical stress behavior should be on the order of 1−2 h.

To briefly summarize, the baseline, back-gated MoS_2 FETs experienced a threshold voltage shift under gate bias stress largely driven by O_2 and H_2O molecules in the ambient air environment. This threshold voltage instability exhibited a linear dependence on the stress voltage and a stretched-exponential dependence on stress time with the majority of the change occurring within the first 2 h of stress but with several hundred millivolts of shift happening within the first few minutes. For many applications of MoS_2 FETs, this bias-induced drifting behavior of the threshold voltage would be unacceptable.

To passivate MoS_2 transistors in an effort to eliminate these deleterious effects of bias stress, we explored the incorporation of four distinct protective barrier layers to cover the exposed MoS_2 channel. Figure 3A illustrates the modified device schematic with the introduction of a passivation layer, and Figure 3B shows several of the actual chips with the central device area covered with a passivation layer. The results of the bias stress test at a fixed V_{GS} = 3 V (as presented for the baseline, nonpassivated device in Figure 2A,B) reveal that some of the passivation layers actually exacerbate the threshold voltage shifts while others ameliorate them (Figure 3C,D). To improve statistical rigor, the experiments shown in Figure 3C,D were repeated on three separate devices on each chip with the final results (mean and standard deviation) summarized in Figure 3E.

Selection of the four capping layers was made to explore distinct deposition and material differences. PMMA was spin-coated and is commonly used as a passivation coating for research-level devices. SU-8 was also spin-coated but is significantly thicker than PMMA and is known for its effective resistance to permeation, including in liquid environments.[51−53] The SiN_x was deposited by plasma-enhanced chemical vapor deposition (PECVD), which introduces potential damage to the MoS_2 during deposition but is also a more standard passivation material for solid-state devices. Finally, Al_2O_3 was grown via atomic layer deposition (ALD), which is a less aggressive reactive environment (compared to PECVD) and allows for precise and comparatively thin film deposition (20 nm in this case). This variety of passivation films allows for insight into which offers the most effective protection of MoS_2 from ambient effects while preserving the

https://dx.doi.org/10.1021/acsami.0c08647
ACS Appl. Mater. Interfaces 2020, 12, 35698−35706

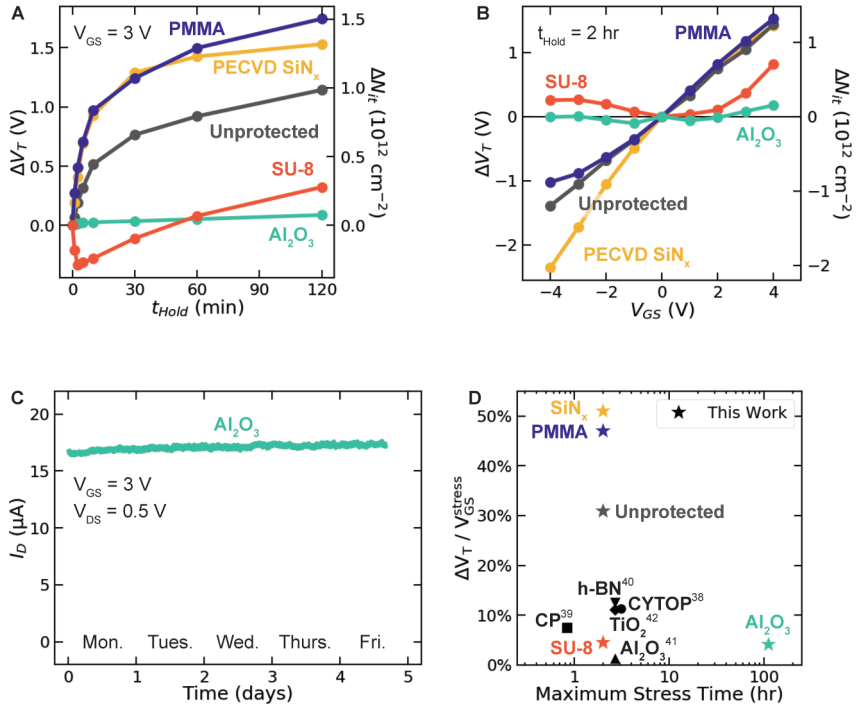

Figure 4. Reduction of trapped charge accumulation by the addition of passivation layers to back-gated MoS_2 FETs and the impact of bias stress time and voltage. (A) Comparison of interface trap accumulation under a variety of passivation layers as a function of bias time and (B) as a function of gate bias voltage. (C) Long-term biasing of MoS_2 FET passivated with Al_2O_3 showing stability over several days. Measurements were captured continuously and saved every 10 s for the entire duration. (D) Benchmarking V_T shift versus maximum stress time against other encapsulation demonstrations for MoS_2 FETs. Percent V_T shift was obtained by normalizing absolute V_T shift by the magnitude of V_{GS} applied during stress. Note that exact device structure and stress conditions vary, but all values are taken for positive V_{GS} stress.

intrinsic MoS_2 electrical properties. Detailed analysis of each capping layer is available in the Supporting Information, including the subthreshold curves for all 76 devices fabricated (Figures S3−S8) and the extraction of any aggregate changes in transconductance, threshold voltage, or subthreshold swing that occurred as a result of encapsulation.

One first point of interest in Figure 3C,D is the relative device current levels at V_{GS} = 3 V. In general, the polymer-capped devices (PMMA and SU-8) displayed slightly higher width-normalized on-current due to a combination of their negative threshold voltage and their ability to sustain high transconductance across a wide voltage range. In contrast, the Al_2O_3-capped device in Figure 3D shows a similar threshold voltage but a more substantial roll-off in transconductance in the on-state, leading to an overall lower current at V_{GS} = 3 V. It is also striking how similar in shape the PMMA-capped response over time is to the baseline unprotected device (Figure 3C), indicating that the PMMA offers no noticeable improvement in device stability. Although the SiN_x-capped device begins at a similar current level to the baseline device, it falls precipitously in a short time and displays the most severe threshold voltage instability. Lastly, both the Al_2O_3-capped and SU-8-capped devices show improvement in stability compared to the baseline with the Al_2O_3 device showing the flattest and most stable response over time (Figure 3C).

The PMMA-capped devices displayed such a large threshold voltage shift in Figure 3D at least in part because the introduction of PMMA caused a distinct permanent negative threshold voltage shift in all devices tested (see Figure S3). As previous reports have indicated, this is because devices susceptible to bias stress instability will tend to shift until $V_T = V_{GS}$.[48,49] Therefore, because the PMMA-capped devices had more negative initial V_T and they were experiencing the same V_{GS} = 3 V during stress as all the other devices in Figure 3C,D, they "had further to go" in a sense and thus experienced a V_T shift that was larger than the baseline unprotected device. Note that if the PMMA had been an effective passivation layer, then we would not have expected to see any threshold voltage shift in Figure 3D, regardless of how negative V_T was to begin with. Exactly why PMMA was unable to prevent molecular adsorption onto the surface of MoS_2 remains unclear, but some researchers have proposed that PMMA films can form pockets of air on the surface of 2D materials,[54] leading to oxidation and degradation of sensitive 2D materials over extended periods of time. This bias-stress performance of PMMA is most comparable to results from p(V4D4-*co*-CHMA) copolymer,[39] which yielded devices that were only slightly more stable than PMMA and with roughly similar threshold voltage and transconductance. Regardless, it is clear that the PMMA provided inadequate protection.

The SiN_x-capped devices also experienced larger V_T shifts under stress, even though their threshold voltages were much closer to the uncapped device (see Figure S5). However, it is important to note that the SiN_x capping layer was deposited by PECVD, during which the MoS_2 was exposed to a 50 W silane plasma for at least the first few seconds of deposition. We expect that this process damaged the MoS_2 crystal structure, and it is possible that having a higher density of surface defects could enhance molecular adsorption during bias stress, as has been previously suggested for oxygen adsorption in particular.[55,56] Enhanced trap filling could account for the higher V_T shifts and the three times steeper drain current settling for SiN_x seen in Figure 3C (see also Figure S15 for comparison of settling time constants). The thickness of 30 nm for our SiN_x

https://dx.doi.org/10.1021/acsami.0c08647
ACS Appl. Mater. Interfaces 2020, 12, 35698−35706

encapsulation was chosen based on another report of encapsulated MoS_2 FETs,[32] but based on these results and more extensive review[57] it now seems most likely that our PECVD tool is incapable of producing such a thin film without any pinhole defects that allow molecular adsorbents to reach the MoS_2 surface.

The results of initial tests in Figure 3 examining V_T shift after 2 h bias-stress intervals were promising for devices capped by either SU-8 photoresist or ALD-grown Al_2O_3. A more rigorous methodology of exploring stress time and voltage was carried out (Figure 4A,B) to examine further differences between the various passivation materials. From the results of Figure 4A, it was discovered that devices capped by SU-8 experienced an initial threshold voltage shift in the opposite direction that was masking an underlying, long-term trend in V_T that is similar to the unmodified devices; that is, the SU-8-capped devices first exhibited an abrupt negative V_T shift over the initial minutes of bias stress, followed by a more gradual positive shift that resulted in a net change after 2 h that was actually rather small (hence, the results of Figure 3C). From Figure 4B, we further see that SU-8 does not follow the linear trend of V_T shifting under increasingly positive gate-stress bias seen in all other devices and shows a net positive V_T shift after 2 h of bias at any voltage. Both of these distinctions in bias stress behavior for the SU-8-passivated devices are attributed to the existence of new and different trap states at the MoS_2−polymer interface. Because the threshold voltage shift is always net positive after 2 h, this means the trap states are filling with net negative charge. This could indicate a different mechanism is taking place, such as the injection of negatively charged hot carriers into the dielectric over the extended duration of bias. Importantly, the behavior observed in Figure 4A for the SU-8-capped device was reversible as the trend was reproduced on the same device.

Despite the unique threshold voltage shifting behavior exhibited by the SU-8-passivated devices, qualitatively they performed quite well and certainly far better than the completely unprotected, PMMA-passivated or SiN_x-passivated devices. Additionally, the spin-coating encapsulation process was facile and had high yield (∼90%), especially compared to the reduced yield observed for devices with ALD Al_2O_3 passivation layers (∼70%). These yield percentages are listed in Table S1 as the "post-capping yield" and were calculated from the number of functioning devices that survived the encapsulation step; hence, this provides an indication of how "risky" each process is for the devices. Devices were determined to fail to survive encapsulation if (1) their on-current reduced to effectively zero or, more commonly, (2) their gate current increased to more than 50 nA. Interestingly, while PECVD SiN_x devices did not perform well, that process had actually very high yield as well (90%), possibly because it was so fast and the devices only spent a couple of minutes in the chamber at elevated temperature (unlike ALD, which takes several hours at 120 °C). The reason this metric is critical for comparing capping layers is that many applications can become prohibitively expensive if yield is compromised too early in the fabrication processes. Importantly, SU-8 stands alone as the only capping layer that substantially improves device stability while also maintaining high yield. Finally, the SU-8 device instabilities were not obvious in Figure 3 and only actually uncovered by the rigorous tests shown in Figure 4; the overall passivation quality is clearly good enough for there to be several reports of SU-8 encapsulation improving the shelf life of air-sensitive thin-film transistors.[58,59] For these reasons, we are optimistic that SU-8 can still be a good choice for most applications.

Another important takeaway from the gate bias-dependent threshold voltage shift data shown in Figure 4B is how consistent the response of the PMMA-passivated and SiN_x-passivated devices are with the unprotected device. This is evidence that the trap mechanisms responsible for V_T instability in the unprotected device remain largely unaffected by these capping layers. While we cannot rule out the introduction of additional traps within the PMMA or SiN_x capping layers, we would not have expected the curves in Figure 4B to match so well if that were the case. The reality may be a combination of both internal traps within the PMMA and SiN_x with molecular adsorption via diffusion still playing a key role through PMMA air pockets or SiN_x pinholes. In contrast, the SU-8 and Al_2O_3 both offer appreciable improvements to the V_T shifting behavior under the varying gate stress magnitude and polarity with the Al_2O_3 offering slightly better protection than the spin-coated polymer. This overall consistency in behavior (PMMA consistent with SiN_x and also SU-8 consistent with Al_2O_3) seen across capping layers that have otherwise such different physical properties (in addition to the evidence from Figure S12 for molecular adsorption as a dominant mechanism) inspires confidence that these results should be more broadly applicable to other 2D material systems in addition to MoS_2. Notably, alumina passivation on black phosphorus (BP) FETs has already been shown to both protect from ambient degradation and to enhance electrical stress stability.[60,61] In addition, tungsten selenide (WSe_2) FETs have been shown to be susceptible to p-type doping from oxygen adsorption.[62] Compared to MoS_2, however, experimental demonstrations of electrical stress in these FETs are much more sparse, and therefore we believe additional study of the specific effect of passivation on stress stability is warranted.

Ultimately, the Al_2O_3-capped devices exhibited the most encouraging stability under all bias stress conditions, demonstrating negligible changes in V_T even after days of continuous bias stress, as shown in Figure 4C. However, as previously noted, it is significant that Al_2O_3 devices showed the lowest post-capping yield, and so this is worth a closer look. A key problem was that any devices capped with Al_2O_3 experienced a substantial negative threshold voltage shift immediately after deposition of the film, making it often impossible to gate the device fully off (see Figure S16). This effect is commonly observed in Al_2O_3-capped devices,[63] and it indicates that the ALD films contain a significant amount of built-in fixed positive charge (such as unsatisfied Al^+ dangling bonds). We found this effect to be most prominent for 40 and 30 nm thick Al_2O_3 films, which is why the devices reported herein were only coated with 20 nm of Al_2O_3. More details can be found in the Supporting Information, and while these effects could potentially be overcome by further process optimization, at present the hampered yield of Al_2O_3-capped devices is a nontrivial cost to its use as a passivation layer. All of this is in contrast to the SU-8-capped devices, which demonstrated close to ideal yield for all devices tested and displayed the next-best electrical stability. Since SU-8 has also further shown compatibility as a passivation layer in biosensors and other liquid environments, it could therefore prove valuable for MoS_2 FETs used in this capacity.[51−53]

A benchmarking comparison of the threshold voltage shift versus bias stress time is provided in Figure 4D. While this

https://dx.doi.org/10.1021/acsami.0c08647
ACS Appl. Mater. Interfaces 2020, 12, 35698−35706

comparison looks only at one aspect of the electrical stability, it does reveal that both the SU-8 and Al_2O_3 provide stability that is on par with the best previously reported approaches and for longer bias stress durations. The overall performance of the Al_2O_3-capped devices is consistent with the one other report[41] of bias stress in an MoS_2 FET. It is notable that Illarionov et al.[41] report pushing their devices to a gate stress field of 4.8 MV/cm, while we were limited to 1.6 MV/cm by some of the large metal features required for wire-bonding our devices (these chip features are even visible to the naked eye in Figure 1F). With metal features of this size, our backside gate oxide was far more susceptible to breakdown if we exceeded a field of 2 MV/cm for hours at a time. While they report higher stress fields, we report more than an order of magnitude longer stress duration, which is an equally important metric, particularly for applications that do not require high voltage. Since we have seen here that stress intensity and duration both contribute to the device response, it is reassuring that our two different approaches produced similar results.

CONCLUSION

In conclusion, we have investigated the bias stress stability of MoS_2 field-effect transistors in ambient air under a variety of stress times and voltage conditions. In uncapped devices, we observed substantial threshold voltage shifts occurring primarily in the first 2 h of stress with the magnitude and polarity of the shift depending linearly on the gate voltage under stress. These effects correlated to changes in interface charge trap density of up to 10^{12} cm^{-2} but were fully reversible and significantly reduced under vacuum or dry nitrogen conditions, leading us to explore several capping layers to protect the devices. Devices capped with PMMA and PECVD SiN_x showed no improvement or even worse electrical stability, while an SU-8 capping layer provided some notable improvement with a facile deposition process and very high device yield. ALD Al_2O_3-capped devices demonstrated the best stability with no observable change in threshold voltage even after 5 days of continuous stress but also showed low device yield after passivation. These results demonstrate the importance of developing a rigorous characterization methodology when evaluating the stability of devices under stress to expose the flaws of unstable devices and the appropriateness of certain passivation layers. Not every capping layer is equally effective for protecting the channel of MoS_2 transistors, but one can be selected with care to produce devices that operate in ambient air with no sign of instability. This shows promise for the continued development and integration of air-stable 2D transistors into future electronic devices and sensors.

ASSOCIATED CONTENT

Supporting Information

The Supporting Information is available free of charge at https://pubs.acs.org/doi/10.1021/acsami.0c08647.

Detailed description of processes used in the fabrication of the MoS_2 FETs, additional electrical characterization of each chip, comparison to multilayer and monolayer devices on 90 nm-SiO_2 substrates, and long-term characterization tests in vacuum and dry nitrogen environments (PDF)

AUTHOR INFORMATION

Corresponding Author

Aaron D. Franklin − *Department of Electrical and Computer Engineering and Department of Chemistry, Duke University, Durham, North Carolina 27708, United States;* orcid.org/0000-0002-1128-9327; Email: aaron.franklin@duke.edu

Authors

James L. Doherty − *Department of Electrical and Computer Engineering, Duke University, Durham, North Carolina 27708, United States;* orcid.org/0000-0003-1571-0622

Steven G. Noyce − *Department of Electrical and Computer Engineering, Duke University, Durham, North Carolina 27708, United States;* orcid.org/0000-0002-2953-7560

Zhihui Cheng − *Department of Electrical and Computer Engineering, Duke University, Durham, North Carolina 27708, United States;* orcid.org/0000-0003-1285-0523

Hattan Abuzaid − *Department of Electrical and Computer Engineering, Duke University, Durham, North Carolina 27708, United States;* orcid.org/0000-0002-6712-4644

Complete contact information is available at: https://pubs.acs.org/10.1021/acsami.0c08647

Author Contributions

J.L.D. and A.D.F. conceived the study. J.L.D. fabricated the devices, designed the experiments, and performed the device measurements. S.G.N. aided in the experimental design. Z.C. and H.A. contributed to device fabrication processes. A.D.F. supervised the research and provided scientific guidance. All authors contributed to the writing of the manuscript.

Notes

The authors declare no competing financial interest.

ACKNOWLEDGMENTS

This work was supported in part by NSF Grant ECCS-1915814 and NIH Grant 1R01HL146849. This work was performed in part at the Duke University Shared Materials Instrumentation Facility (SMIF), which is a member of the North Carolina Research Triangle Nanotechnology Network (RTNN), which is supported by the National Science Foundation (Grant ECCS-1542015) as part of the National Nanotechnology Coordinated Infrastructure (NNCI).

REFERENCES

(1) Franklin, A. D. Nanomaterials in Transistors: From High-Performance to Thin-Film Applications. *Science* **2015**, *349*, aab2750.

(2) Novoselov, K. S.; Mishchenko, A.; Carvalho, A.; Castro Neto, A. H. 2D Materials and Van der Waals Heterostructures. *Science* **2016**, *353*, aac9439.

(3) Radisavljevic, B.; Radenovic, A.; Brivio, J.; Giacometti, V.; Kis, A. Single-layer MoS_2 Transistors. *Nat. Nanotechnol.* **2011**, *6*, 147−150.

(4) Desai, S. B.; Madhvapathy, S. R.; Sachid, A. B.; Llinas, J. P.; Wang, Q.; Ahn, G. H.; Pitner, G.; Kim, M. J.; Bokor, J.; Hu, C.; Wong, H.-S. P.; Javey, A. MoS_2 Transistors with 1-Nanometer Gate Lengths. *Science* **2016**, *354*, 99−102.

(5) Liu, H.; Neal, A. T.; Ye, P. D. Channel Length Scaling of MoS_2 MOSFETs. *ACS Nano* **2012**, *6*, 8563−8569.

(6) Su, Y.; Kshirsagar, C. U.; Robbins, M. C.; Haratipour, N.; Koester, S. J. Symmetric Complementary Logic Inverter Using Integrated Black Phosphorus and MoS_2 Transistors. *2D Mater.* **2016**, *3*, No. 011006.

(7) Das, S.; Chen, H.-Y.; Penumatcha, A. V.; Appenzeller, J. High Performance Multilayer MoS_2 Transistors with Scandium Contacts. *Nano Lett.* **2013**, *13*, 100−105.

(8) Liu, Y.; Guo, J.; Wu, Y.; Zhu, E.; Weiss, N. O.; He, Q.; Wu, H.; Cheng, H. C.; Xu, Y.; Shakir, I.; Huang, Y.; Duan, X. Pushing the Performance Limit of Sub-100 nm Molybdenum Disulfide Transistors. *Nano Lett.* **2016**, *16*, 6337−6342.
(9) Cheng, Z.; Price, K.; Franklin, A. D. Contacting and Gating 2-D Nanomaterials. *IEEE Trans. Electron Devices* **2018**, *65*, 4073−4083.
(10) Cui, X.; Lee, G. H.; Kim, Y. D.; Arefe, G.; Huang, P. Y.; Lee, C. H.; Chenet, D. A.; Zhang, X.; Wang, L.; Ye, F.; Pizzocchero, F.; Jessen, B. S.; Watanabe, K.; Taniguchi, T.; Muller, D. A.; Low, T.; Kim, P.; Hone, J. Multi-Terminal Transport Measurements of MoS_2 Using a Van der Waals Heterostructure Device Platform. *Nat. Nanotechnol.* **2015**, *10*, 534−540.
(11) Liu, Y.; Wu, H.; Cheng, H.-C.; Yang, S.; Zhu, E.; He, Q.; Ding, M.; Li, D.; Guo, J.; Weiss, N. O.; Huang, Y.; Duan, X. Toward Barrier Free Contact to Molybdenum Disulfide Using Graphene Electrodes. *Nano Lett.* **2015**, *15*, 3030−3034.
(12) Najmaei, S.; Zou, X.; Er, D.; Li, J.; Jin, Z.; Gao, W.; Zhang, Q.; Park, S.; Ge, L.; Lei, S.; Kono, J.; Shenoy, V. B.; Yakobson, B. I.; George, A.; Ajayan, P. M.; Lou, J. Tailoring the Physical Properties of Molybdenum Disulfide Monolayers by Control of Interfacial Chemistry. *Nano Lett.* **2014**, *14*, 1354−1361.
(13) Bao, W.; Cai, X.; Kim, D.; Sridhara, K.; Fuhrer, M. S. High Mobility Ambipolar MoS_2 Field-Effect Transistors: Substrate and Dielectric Effects. *Appl. Phys. Lett.* **2013**, *102*, No. 042104.
(14) Bolshakov, P.; Zhao, P.; Azcatl, A.; Hurley, P. K.; Wallace, R. M.; Young, C. D. Improvement in Top-Gate MoS_2 Transistor Performance Due to High Quality Backside Al_2O_3 Layer. *Appl. Phys. Lett.* **2017**, *111*, No. 032110.
(15) Radisavljevic, B.; Kis, A. Mobility Engineering and a Metal-Insulator Transition in Monolayer MoS_2. *Nat. Mater.* **2013**, *12*, 815−820.
(16) Zou, X.; Wang, J.; Chiu, C.-H.; Wu, Y.; Xiao, X.; Jiang, C.; Wu, W.-W.; Mai, L.; Chen, T.; Li, J.; Ho, J. C.; Liao, L. Interface Engineering for High-Performance Top-Gated MoS_2 Field-Effect Transistors. *Adv. Mater.* **2014**, *26*, 6255−6261.
(17) Li, X.; Xiong, X.; Li, T.; Li, S.; Zhang, Z.; Wu, Y. Effect of Dielectric Interface on the Performance of MoS_2 Transistors. *ACS Appl. Mater. Interfaces* **2017**, *9*, 44602−44608.
(18) Lee, G. H.; Cui, X.; Kim, Y. D.; Arefe, G.; Zhang, X.; Lee, C. H.; Ye, F.; Watanabe, K.; Taniguchi, T.; Kim, P.; Hone, J. Highly Stable, Dual-Gated MoS_2 Transistors Encapsulated by Hexagonal Boron Nitride with Gate-Controllable Contact, Resistance, and Threshold Voltage. *ACS Nano* **2015**, *9*, 7019−7026.
(19) Yu, Z.; Pan, Y.; Shen, Y.; Wang, Z.; Ong, Z.-Y.; Xu, T.; Xin, R.; Pan, L.; Wang, B.; Sun, L.; Wang, J.; Zhang, G.; Zhang, Y. W.; Shi, Y.; Wang, X. Towards Intrinsic Charge Transport in Monolayer Molybdenum Disulfide by Defect and Interface Engineering. *Nat. Commun.* **2014**, *5*, 5290.
(20) Yu, Z.; Ong, Z.-Y.; Pan, Y.; Cui, Y.; Xin, R.; Shi, Y.; Wang, B.; Wu, Y.; Chen, T.; Zhang, Y.-W.; Zhang, G.; Wang, X. Realization of Room-Temperature Phonon-Limited Carrier Transport in Monolayer MoS_2 by Dielectric and Carrier Screening. *Adv. Mater.* **2016**, *28*, 547−552.
(21) Liu, T.; Liu, S.; Tu, K. H.; Schmidt, H.; Chu, L.; Xiang, D.; Martin, J.; Eda, G.; Ross, C. A.; Garaj, S. Crested Two-Dimensional Transistors. *Nat. Nanotechnol.* **2019**, *14*, 223−226.
(22) Tsai, M. L.; Su, S. H.; Chang, J. K.; Tsai, D. S.; Chen, C. H.; Wu, C. I.; Li, L. J.; Chen, L. J.; He, J. H. Monolayer MoS_2 Heterojunction Solar Cells. *ACS Nano* **2014**, *8*, 8317−8322.
(23) Pezeshki, A.; Shokouh, S. H. H.; Nazari, T.; Oh, K.; Im, S. Electric and Photovoltaic Behavior of a Few-Layer α-$MoTe_2$/MoS_2 Dichalcogenide Heterojunction. *Adv. Mater.* **2016**, *28*, 3216−3222.
(24) Sangwan, V. K.; Lee, H. S.; Bergeron, H.; Balla, I.; Beck, M. E.; Chen, K. S.; Hersam, M. C. Multi-Terminal Memtransistors from Polycrystalline Monolayer Molybdenum Disulfide. *Nature* **2018**, *554*, 500−504.
(25) Bertolazzi, S.; Krasnozhon, D.; Kis, A. Nonvolatile Memory Cells Based on MoS2/Graphene Heterostructures. *ACS Nano* **2013**, *7*, 3246−3252.
(26) Liu, B.; Chen, L.; Liu, G.; Abbas, A. N.; Fathi, M.; Zhou, C. High-Performance Chemical Sensing Using Schottky-Contacted Chemical Vapor Deposition Grown Monolayer MoS_2 Transistors. *ACS Nano* **2014**, *8*, 5304−5314.
(27) Perkins, F. K.; Friedman, A. L.; Cobas, E.; Campbell, P. M.; Jernigan, G. G.; Jonker, B. T. Chemical Vapor Sensing with Monolayer MoS_2. *Nano Lett.* **2013**, *13*, 668−673.
(28) Late, D. J.; Huang, Y. K.; Liu, B.; Acharya, J.; Shirodkar, S. N.; Luo, J.; Yan, A.; Charles, D.; Waghmare, U. V.; Dravid, V. P.; Rao, C. N. R. Sensing Behavior of Atomically Thin-Layered MoS_2 Transistors. *ACS Nano* **2013**, *7*, 4879−4891.
(29) Jiang, J.; Dhar, S. Tuning the Threshold Voltage from Depletion to Enhancement Mode in a Multilayer MoS_2 Transistor via Oxygen Adsorption and Desorption. *Phys. Chem. Chem. Phys.* **2016**, *18*, 685−689.
(30) Shu, J.; Wu, G.; Gao, S.; Liu, B.; Wei, X.; Chen, Q. Influence of Water Vapor on the Electronic Property of MoS_2 Field Effect Transistors. *Nanotechnology* **2017**, *28*, 204003.
(31) Ahn, J. H.; Parkin, W. M.; Naylor, C. H.; Johnson, A. T. C.; Drndić, M. Ambient Effects on Electrical Characteristics of CVD-Grown Monolayer MoS_2 Field-Effect Transistors. *Sci. Rep.* **2017**, *7*, 4075.
(32) Late, D. J.; Liu, B.; Matte, H. S. S. R.; Dravid, V. P.; Rao, C. N. R. Hysteresis in Single-Layer MoS_2 Field Effect Transistors. *ACS Nano* **2012**, *6*, 5635−5641.
(33) Shimazu, Y.; Tashiro, M.; Sonobe, S.; Takahashi, M. Environmental Effects on Hysteresis of Transfer Characteristics in Molybdenum Disulfide Field-Effect Transistors. *Sci. Rep.* **2016**, *6*, 30084.
(34) Di Bartolomeo, A.; Genovese, L.; Giubileo, F.; Iemmo, L.; Luongo, G.; Foller, T.; Schleberger, M. Hysteresis in the Transfer Characteristics of MoS_2 Transistors. *2D Mater.* **2018**, *5*, No. 015014.
(35) Li, T.; Du, G.; Zhang, B.; Zeng, Z. Scaling Behavior of Hysteresis in Multilayer MoS_2 Field Effect Transistors. *Appl. Phys. Lett.* **2014**, *105*, No. 093107.
(36) Guo, Y.; Wei, X.; Shu, J.; Liu, B.; Yin, J.; Guan, C.; Han, Y.; Gao, S.; Chen, Q. Charge Trapping at the MoS_2-SiO_2 Interface and its Effects on the Characteristics of MoS_2 Metal-Oxide-Semiconductor Field Effect Transistors. *Appl. Phys. Lett.* **2015**, *106*, 103109.
(37) Cho, K.; Park, W.; Park, J.; Jeong, H.; Jang, J.; Kim, T. Y.; Hong, W. K.; Hong, S.; Lee, T. Electric Stress-Induced Threshold Voltage Instability of Multilayer MoS_2 Field Effect Transistors. *ACS Nano* **2013**, *7*, 7751−7758.
(38) Seo, S. G.; Jin, S. H. Bias Temperature Stress Instability of Multilayered MoS_2 Field-Effect Transistors With CYTOP Passivation. *IEEE Trans. Electron Devices* **2019**, *66*, 2208−2213.
(39) Kim, M. J.; Choi, Y.; Seok, J.; Lee, S.; Kim, Y. J.; Lee, J. Y.; Cho, J. H. Defect-Free Copolymer Gate Dielectrics for Gating MoS_2 Transistors. *J. Phys. Chem. C* **2018**, *122*, 12193−12199.
(40) Illarionov, Y. Y.; Rzepa, G.; Waltl, M.; Knobloch, T.; Grill, A.; Furchi, M. M.; Mueller, T.; Grasser, T. The Role of Charge Trapping in MoS_2/SiO_2 and MoS_2/hBN Field-Effect Transistors. *2D Mater.* **2016**, *3*, No. 035004.
(41) Illarionov, Y. Y.; Smithe, K. K. H.; Waltl, M.; Knobloch, T.; Pop, E.; Grasser, T. Improved Hysteresis and Reliability of MoS_2 Transistors with High-Quality CVD Growth and Al_2O_3 Encapsulation. *IEEE Electron Device Lett.* **2017**, *38*, 1763−1766.
(42) Park, W.; Pak, Y.; Jang, H. Y.; Nam, J. H.; Kim, T. H.; Oh, S.; Choi, S. M.; Kim, Y.; Cho, B. Improvement of the Bias Stress Stability in 2D MoS_2 and WS_2 transistors with a TiO_2 Interfacial Layer. *Nanomaterials* **2019**, *9*, 1155.
(43) Cheng, Z.; Cardenas, J. A.; McGuire, F.; Najmaei, S.; Franklin, A. D. Modifying the Ni-MoS_2 Contact Interface Using a Broad-Beam Ion Source. *IEEE Electron Device Lett.* **2016**, *37*, 1234−1237.
(44) McGuire, F. A.; Lin, Y.-C.; Price, K.; Rayner, G. B.; Khandelwal, S.; Salahuddin, S.; Franklin, A. D. Sustained Sub-60 mV/decade Switching Via the Negative Capacitance Effect in MoS_2 Transistors. *Nano Lett.* **2017**, *17*, 4801−4806.

https://dx.doi.org/10.1021/acsami.0c08647
ACS Appl. Mater. Interfaces 2020, 12, 35698−35706

(45) Noyce, S. G.; Doherty, J. L.; Cheng, Z.; Han, H.; Bowen, S.; Franklin, A. D. Electronic Stability of Carbon Nanotube Transistors Under Long-Term Bias Stress. *Nano Lett.* **2019**, *19*, 1460−1466.
(46) Yang, S.; Park, S.; Jang, S.; Kim, H.; Kwon, J. Y. Electrical Stability of Multilayer MoS_2 Field-Effect Transistor Under Negative Bias Stress at Various Temperatures. *Phys. Status Solidi RRL* **2014**, *8*, 714−718.
(47) Lee, J. M.; Cho, I. T.; Lee, J. H.; Kwon, H. I. Bias-Stress-Induced Stretched-Exponential Time Dependence of Threshold Voltage Shift in InGaZnO Thin Film Transistors. *Appl. Phys. Lett.* **2008**, *93*, No. 093504.
(48) Chen, T. C.; Chang, T. C.; Tsai, C. T.; Hsieh, T. Y.; Chen, S. C.; Lin, C. S.; Hung, M. C.; Tu, C. H.; Chang, J. J.; Chen, P. L. Behaviors of InGaZnO Thin Film Transistor Under Illuminated Positive Gate-Bias Stress. *Appl. Phys. Lett.* **2010**, *97*, 112104.
(49) Mathijssen, S. G. J.; Cölle, M.; Gomes, H.; Smits, E. C. P.; De Boer, B.; McCulloch, I.; Bobbert, P. A.; De Leeuw, D. M. Dynamics of Threshold Voltage Shifts in Organic and Amorphous Silicon Field-Effect Transistors. *Adv. Mater.* **2007**, *19*, 2785−2789.
(50) Mathijssen, S. G. J.; Kemerink, M.; Sharma, A.; Cölle, M.; Bobbert, P. A.; Janssen, R. A. J.; De Leeuw, D. M. Charge Trapping at the Dielectric of Organic Transistors Visualized in Real Time and Space. *Adv. Mater.* **2008**, *20*, 975−979.
(51) Lee, D. W.; Lee, J.; Sohn, I. Y.; Kim, B. Y.; Son, Y. M.; Bark, H.; Jung, J.; Choi, M.; Kim, T. H.; Lee, C.; Lee, N. E. Field-Effect Transistor with a Chemically Synthesized MoS_2 Sensing Channel for Label-Free and Highly Sensitive Electrical Detection of DNA Hybridization. *Nano Res.* **2015**, *8*, 2340−2350.
(52) Hammond, P. A.; Cumming, D. R. S. Encapsulation of a Liquid-Sensing Microchip Using SU-8 Photoresist. *Microelectron. Eng.* **2004**, *73*−*74*, 893−897.
(53) Dankerl, M.; Hauf, M. V.; Lippert, A.; Hess, L. H.; Birner, S.; Sharp, I. D.; Mahmood, A.; Mallet, P.; Veuillen, J. Y.; Stutzmann, M.; Garrido, J. A. Graphene Solution-Gated Field-Effect Transistor Array for Sensing Applications. *Adv. Funct. Mater.* **2010**, *20*, 3117−3124.
(54) Thi, Q. H.; Kim, H.; Zhao, J.; Ly, T. H. Coating Two-Dimensional MoS_2 with Polymer Creates a Corrosive Non-Uniform Interface. *2D Mater. Appl.* **2018**, *2*, 34.
(55) Park, W.; Park, J.; Jang, J.; Lee, H.; Jeong, H.; Cho, K.; Hong, S.; Lee, T. Oxygen Environmental and Passivation Effects on Molybdenum Disulfide Field Effect Transistors. *Nanotechnology* **2013**, *24*, No. 095202.
(56) Qiu, H.; Pan, L.; Yao, Z.; Li, J.; Shi, Y.; Wang, X. Electrical Characterization of Back-Gated Bi-layer MoS_2 Field-Effect Transistors and the Effect of Ambient on their Performances. *Appl. Phys. Lett.* **2012**, *100*, 123104.
(57) Engelhardt, J.; Hahn, G.; Terheiden, B. Multifunctional ICP-PECVD Silicon Nitride Layers for High-efficiency Silicon Solar Cell Applications. *Energy Procedia* **2015**, *77*, 786−790.
(58) Olziersky, A.; Barquinha, P.; Vila, A.; Pereira, L.; Goncalves, G.; Fortunato, E.; Martins, R.; Morante, J. R. Insight on the SU-8 Resist as Passivation Layer for Transparent Ga_2O_3-In_2O_3-ZnO Thin-Film Transistors. *J. Appl. Phys.* **2010**, *108*, No. 064505.
(59) Han, Y. J.; Choi, Y. J.; Cho, I. T.; Jin, S. H.; Lee, J. H.; Kwon, H. I. Improvement of Long-Term Durability and Bias Stress Stability in p-Type SnO Thin-Film Transistors Using a SU-8 Passivation Layer. *IEEE Electron Device Lett.* **2014**, *35*, 1260−1262.
(60) Illarionov, Y. Y.; Waltl, M.; Rzepa, G.; Kim, J. S.; Kim, S.; Dodabalapur, A.; Akinwande, D.; Grasser, T. Long-Term Stability and Reliability of Black Phosphorus Field-Effect Transistors. *ACS Nano* **2016**, *10*, 9543−9549.
(61) Wood, J. D.; Wells, S. A.; Jariwala, D.; Chen, K. S.; Cho, E.; Sangwan, V. K.; Liu, X.; Lauhon, L. J.; Marks, T. J.; Hersam, M. C. Effective Passivation of Exfoliated Black Phosphorus Transistors Against Ambient Degradation. *Nano Lett.* **2014**, *14*, 6964−6970.
(62) Wang, S.; Zhao, W.; Giustiniano, F.; Eda, G. Effect of Oxygen and Ozone on P-Type Doping of Ultra-Thin WSe_2 and $MoSe_2$ Field Effect Transistors. *Phys. Chem. Chem. Phys.* **2016**, *18*, 4304−4309.
(63) Song, J. G.; Kim, S. J.; Woo, W. J.; Kim, Y.; Oh, I. K.; Ryu, G. H.; Lee, Z.; Lim, J. H.; Park, J.; Kim, H. Effect of Al_2O_3 Deposition on Performance of Top-Gated Monolayer MoS_2-Based Field Effect Transistor. *ACS Appl. Mater. Interfaces* **2016**, *8*, 28130−28135.

https://dx.doi.org/10.1021/acsami.0c08647
ACS Appl. Mater. Interfaces 2020, 12, 35698−35706